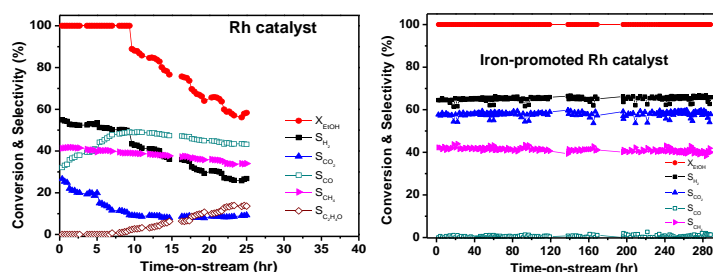




## Contents

**Carbon monoxide-free hydrogen production via low-temperature steam reforming of ethanol over iron-promoted Rh catalyst** pp 197–200

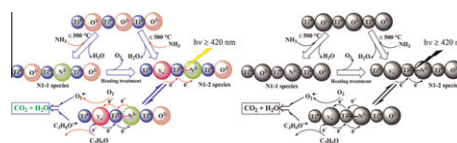
Luwei Chen\*, Catherine Kai Shin Choong, Ziyi Zhong, Lin Huang, Thiam Peng Ang, Liang Hong, Jianyi Lin



For the first time, a novel iron-promoted Rh catalyst is found to produce CO-free H<sub>2</sub> through steam reforming of ethanol at a low temperature ranging between 623 and 673 K.

**Nitrogen-doped titanium dioxide visible light photocatalyst: Spectroscopic identification of photoactive centers** pp 201–214

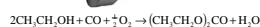
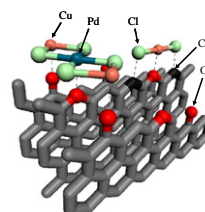
Zizhong Zhang, Xuxu Wang, Jinlin Long\*, Quan Gu, Zhengxin Ding, Xianzhi Fu\*



The nitridation of TiO<sub>2</sub> by NH<sub>3</sub>-generated substitutional N species with a diamagnetic [O–Ti<sup>4+</sup>–N<sup>3–</sup>–Ti<sup>4+</sup>] core stabilized by a neighboring oxygen vacancy that can work under visible light.

**Effects of support composition and pretreatment on the activity and selectivity of carbon-supported PdCu<sub>n</sub>Cl<sub>x</sub> catalysts for the synthesis of diethyl carbonate** pp 215–228

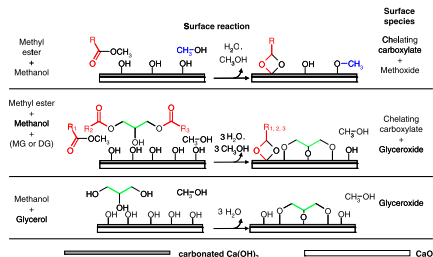
Daniel N. Briggs, Gerry Bong, Eric Leong, Kevin Oei, Gabriella Lestari, Alexis T. Bell\*



PdCu<sub>n</sub>Cl<sub>x</sub> species dispersed on carbon supports catalyze the oxidative carbonylation of ethanol to diethyl carbonate (DEC). Catalyst activity and selectivity are improved by oxidation of the carbon support before preparation, and catalyst stability can be achieved by the addition of ppm levels of CCl<sub>4</sub> into the feed. It is proposed that the highest activity is exhibited by Cl-bridged [CuCl<sub>2</sub>]Pd[CuCl<sub>2</sub>] species.

## Surface chemical promotion of Ca oxide catalysts in biodiesel production reaction by the addition of monoglycerides, diglycerides and glycerol pp 229–236

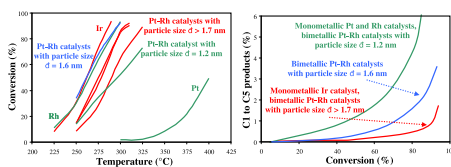
M. López Granados\*, A.C. Alba-Rubio, F. Vila, D. Martín Alonso, R. Mariscal



The reaction to produce biodiesel catalysed by Ca oxide can be strongly promoted by the formation of very active surface Ca glyceroxide if in the initial reactant mixture tenths of mg of MG and/or DG and/or glycerol are present.

## Relationship between the structural properties of supported bimetallic Pt–Rh catalysts and their performances for methylcyclopentane ring opening pp 237–248

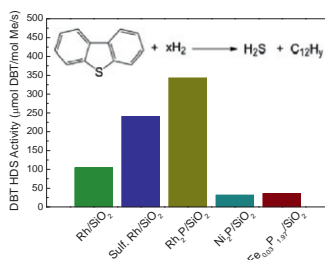
P. Samoila, M. Boutzeloit, C. Espécel\*, F. Epron, P. Marécot



The aim of this study was to characterize in depth supported bimetallic Pt–Rh samples prepared by various routes in order to understand the relationship between their structural properties and their catalytic performances for the methylcyclopentane (MCP) ring opening (RO) under pressure. The largest bimetallic particles ( $d > 1.7$  nm) were the most selective for MCP RO, leading to performances similar to those of iridium-based reference catalysts.

## Hydrodesulfurization properties of rhodium phosphide: Comparison with rhodium metal and sulfide catalysts pp 249–258

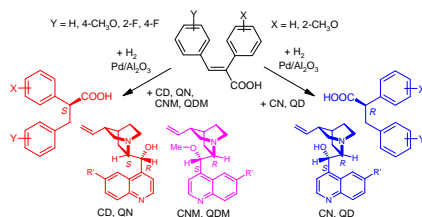
John R. Hayes, Richard H. Bowker, Amy F. Gaudette, Mica C. Smith, Cameron E. Moak, Charles Y. Nam, Thomas K. Pratum, Mark E. Bussell\*



5 wt% Rh<sub>2</sub>P/SiO<sub>2</sub> catalysts were observed to have higher dibenzothiophene hydrodesulfurization activities than Rh/SiO<sub>2</sub> and sulfided Rh/SiO<sub>2</sub> catalysts. The Rh<sub>2</sub>P/SiO<sub>2</sub> catalysts exhibit excellent stability and are more S tolerant than Rh/SiO<sub>2</sub> catalysts.

## Cinchona methyl ethers as modifiers in the enantioselective hydrogenation of (*E*)-2,3-diphenylpropenoic acids over Pd catalyst pp 259–267

György Szöllösi\*, Beáta Hermán, Ferenc Fülöp, Mihály Bartók

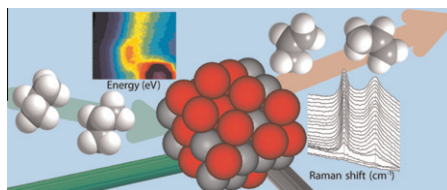


The enantioselective hydrogenation of (*E*)-2,3-diphenylpropenoic acids over Pd/Al<sub>2</sub>O<sub>3</sub> modified by (R)<sup>8</sup>–(S)<sup>9</sup> cinchona methyl ethers resulted in the inversion of the sense of the enantioselectivity. The phenomenon was interpreted by reshaping of the surface chiral sites coupled with a weak and flexible monodentate acid–cinchona ether interaction.

## A combined in situ time-resolved UV–Vis, Raman and high-energy resolution X-ray absorption spectroscopy study on the deactivation behavior of Pt and Pt–Sn propane dehydrogenation catalysts under industrial reaction conditions

pp 268–279

Ana Iglesias-Juez, Andrew M. Beale, Karin Maaijen, Tsu Chien Weng, Pieter Glatzel, Bert M. Weckhuysen\*

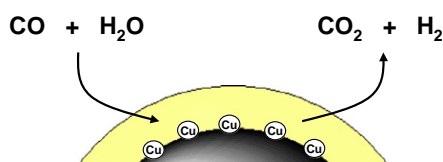


XANES and Raman reveal new information on the properties of supported Pt–Sn nanoparticles during propane dehydrogenation–regeneration cycles leading to insight into the dynamics of Pt–Sn alloy formation at elevated temperatures.

## Water–gas shift catalysts based on ionic liquid mediated supported Cu nanoparticles

pp 280–291

Richard Knapp, Sonja A. Wyrzgol, Andreas Jentys\*, Johannes A. Lercher

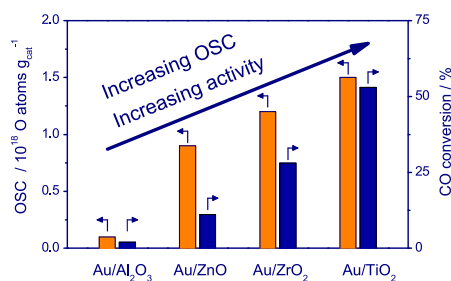


Catalysts coated with suitable ionic liquids show exceptionally high activities for water–gas shift at low temperatures due to weakened interactions with the reactants and products.

## Support effects in the Au-catalyzed CO oxidation – Correlation between activity, oxygen storage capacity, and support reducibility

pp 292–305

D. Widmann, Y. Liu, F. Schüth, R.J. Behm\*

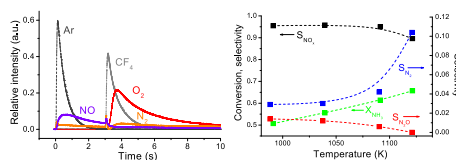


We demonstrate a clear correlation between the oxygen storage capacity (OSC) and the activity for CO oxidation for four different oxide-supported gold catalysts, which differ in the reducibility of the oxide but have similar Au loadings and Au particle sizes. This points to a direct participation of the support in the reaction, confirming the earlier qualitative concept of ‘active’ and ‘inert’ oxides.

## The reaction mechanism of the high temperature ammonia oxidation to nitric oxide over LaCoO<sub>3</sub>

pp 306–313

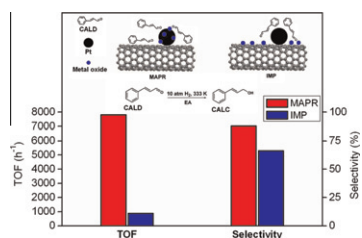
Gregory Biausque, Yves Schuurman\*



By combining different transient (TAP, oxygen exchange) and steady-state techniques, a reaction mechanism for ammonia oxidation over LaCoO<sub>3</sub> has been proposed.

## Carbon nanotube-supported Pt-based bimetallic catalysts prepared by a microwave-assisted polyol reduction method and their catalytic applications in the selective hydrogenation pp 314–326

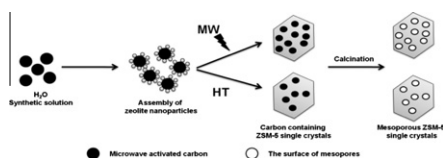
Zhen Guo, Yuanting Chen, Lusi Li, Xiaoming Wang, Gary L. Haller, Yanhui Yang\*



CNT-supported Pt bimetallic catalysts synthesized by microwave-assisted polyol reduction method outperform the corresponding impregnated catalysts in cinnamaldehyde hydrogenation, which is attributed to the close contact between Pt and promoter.

## Direct synthesis of carbon-templating mesoporous ZSM-5 using microwave heating pp 327–334

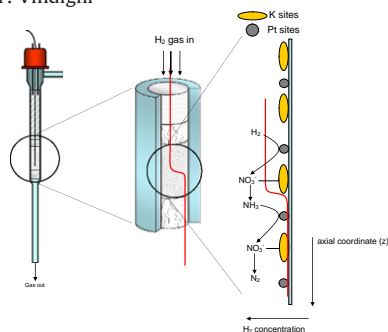
Jeong-Boon Koo, Nanzhe Jiang, Shunmugavel Saravanamurugan, Martina Bejblová, Zuzana Musilová, Jiří Čejka\*, Sang-Eon Park\*



Carbon-templated mesoporous ZSM-5 have been synthesized by microwave irradiation. The nature of acid sites both in the micropores and on the surface of mesopores was investigated by in situ FTIR.

## The NO<sub>x</sub> storage-reduction on Pt–K/Al<sub>2</sub>O<sub>3</sub> Lean NO<sub>x</sub> Trap catalyst pp 335–350

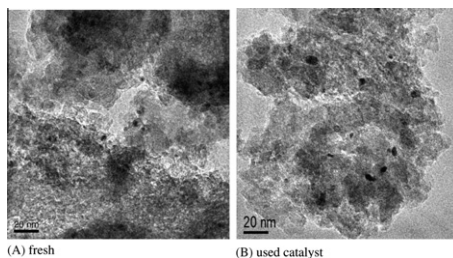
L. Castoldi, L. Lietti\*, P. Forzatti, S. Morandi, G. Ghiotti, F. Vindigni



The “H<sub>2</sub> front” model for the reduction of the stored NO<sub>x</sub> over Pt–K/Al<sub>2</sub>O<sub>3</sub> catalyst.

## Designing Pt nanoparticles supported on CeO<sub>2</sub>–Al<sub>2</sub>O<sub>3</sub>: Synthesis, characterization and catalytic properties in the steam reforming and partial oxidation of methane pp 351–359

P.J.S. Prieto, A.P. Ferreira, P.S. Haddad, D. Zanchet\*, J.M.C. Bueno\*

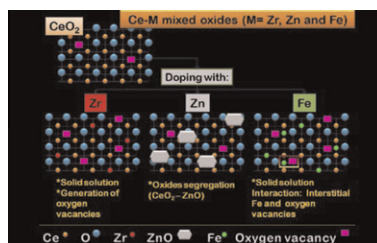


Catalyst synthesized from Pt nanoparticles of uniform size (Pt-NPs) well dispersed on CeO<sub>2</sub>–Al<sub>2</sub>O<sub>3</sub> supports shows high stability under methane oxyforming reactions.

**Gold supported on metal-doped ceria catalysts (M = Zr, Zn and Fe) for the preferential oxidation of CO (PROX)**

pp 360–370

O.H. Laguna\*, F. Romero Sarria, M.A. Centeno, J.A. Odriozola

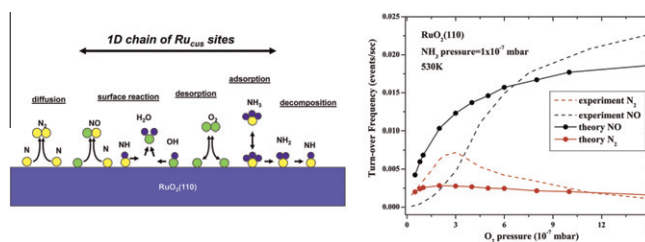


The doping CeO<sub>2</sub> with Zr, Zn and Fe was studied. Doping with Zr or Fe resulted in solid solution, while doping with Zn resulted in the surface segregation of ZnO. The formation of oxygen vacancies is enhanced with Zr, remains constant with Zn and disappears on doping with Fe.

**Selective oxidation of ammonia on RuO<sub>2</sub>(1 1 0): A combined DFT and KMC study**

pp 371–381

Sampyo Hong, Altaf Karim, Talat S. Rahman\*, Karl Jacobi, Gerhard Ertl

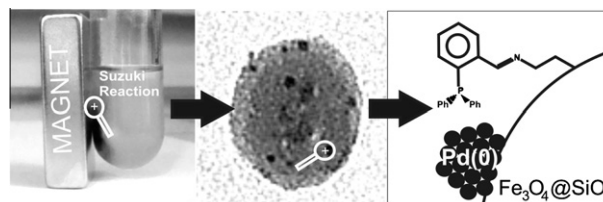


*Ab initio* Kinetic Monte Carlo (KMC) simulations of 18 reactions for the selective oxidation of ammonia on RuO<sub>2</sub>(1 1 0) show 93% selectivity for NO, in close agreement with experiment (~95%).

**A single-step procedure for the preparation of palladium nanoparticles and a phosphine-functionalized support as catalyst for Suzuki cross-coupling reactions**

pp 382–389

Natália J.S. Costa, Pedro K. Kiyohara, Adriano L. Monteiro, Yannick Coppel, Karine Philippot, Liane M. Rossi\*

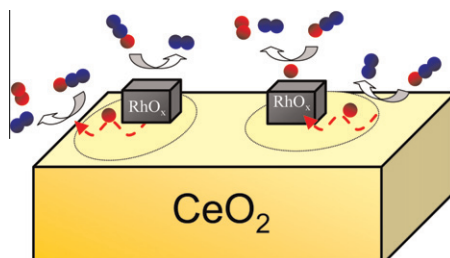


Magnetically recoverable supported Pd nanoparticles stabilized by pendant phosphine groups exhibited good activity and high selectivity in Suzuki cross-coupling reaction.

**Study by isotopic gases and *in situ* spectroscopies (DRIFTS, XPS and Raman) of the N<sub>2</sub>O decomposition mechanism on Rh/CeO<sub>2</sub> and Rh/ $\gamma$ -Al<sub>2</sub>O<sub>3</sub> catalysts**

pp 390–401

S. Parres-Esclapez, I. Such-Basañez, M.J. Illán-Gómez, C. Salinas-Martínez de Lecea, A. Bueno-López\*

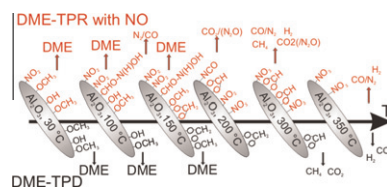


The higher catalytic activity for N<sub>2</sub>O decomposition of Rh/CeO<sub>2</sub> in comparison to Rh/ $\gamma$ -Al<sub>2</sub>O<sub>3</sub> is related to the Rh–CeO<sub>2</sub> interaction and to the participation of the CeO<sub>2</sub> support in the N<sub>2</sub>O decomposition mechanism,  $\gamma$ -Al<sub>2</sub>O<sub>3</sub> being an inert carrier.

**Mechanistic aspects of the selective catalytic reduction of NO<sub>x</sub> by dimethyl ether and methanol over  $\gamma$ -Al<sub>2</sub>O<sub>3</sub>**

pp 402–411

Stefanie Tamm\*, Hanna H. Ingelsten, Magnus Skoglundh, Anders E.C. Palmqvist

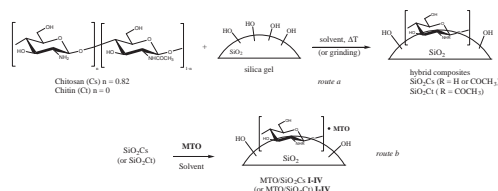


Alumina is a promising catalyst for the selective catalytic reduction of NO<sub>x</sub> with dimethyl ether (DME), an energy effective alternative fuel. A correlation of the surface species with the gas composition allows proposing the relevant surface reactions during DME-SCR.

**Chitin- and chitosan-anchored methyltrioxorhenium: An innovative approach for selective heterogeneous catalytic epoxidations of olefins**

pp 412–422

Andrea Di Giuseppe, Marcello Crucianelli\*, Maurizio Passacantando, Stefano Nisi, Raffaele Saladino\*

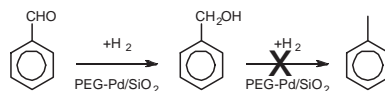


Novel complexes between methyltrioxorhenium (MTO) and natural polysaccharides like chitin, chitosan, modified chitosan, and silica-polysaccharide hybrid composites were synthesized and used as efficient heterogeneous catalysts for the selective oxidation of alkenes, with urea hydrogen peroxide complex (UHP) as primary oxidant.

**Polymers as novel modifiers for supported metal catalyst in hydrogenation of benzaldehydes**

pp 423–428

Masaki Okamoto\*, Tomoyuki Hirao, Tatsuya Yamaai



Modification of a supported palladium metal catalyst with polyethylene glycol as a novel modifier improved catalytic activity and selectivity for partial hydrogenated products in vapor-phase hydrogenations of benzaldehyde and isoprene.